Supplementary information:

Symmetry-resolved Raman fingerprints of uniaxial and biaxial strain in WSe_2

Mariana M. Gomes[1,2*], Pablo Ares[1,2,3], Andres Castellanos-Gomez[4], Carmen Munuera[4], Álvaro Rodríguez[1,2,4 *]

[1]Departamento de Física de la Materia Condensada, Universidad Autónoma de Madrid, Madrid, 28049, Spain.
[2]Condensed Matter Physics Center (IFIMAC), Universidad Autónoma de Madrid, Madrid, 28049, Spain.
[3]Instituto Nicolás Cabrera (INC), Universidad Autónoma de Madrid, Madrid, 28049, Spain.
[4]2D Foundry group, Instituto de Ciencia de Materiales de Madrid (ICMM-CSIC), C. Sor Juana Inés de la Cruz, 3, Madrid, 28049, Spain.

*Corresponding author(s): alvaro.rodriguezr@uam.es, mariana.mgomes@uam.es

This Supplementary Information provides the symmetry analysis and additional experimental data supporting the polarization-resolved Raman identification of uniaxial and biaxial strain in WSe_2.

Table of contents:

Supplementary Note 1. Identification of number of layers and description of straining setups.

Supplementary Note 2. Symmetry framework and Raman selection rules.

Supplementary Note 3. Additional strain-dependent unpolarized Raman measurements for 1-3L WSe_2.

Supplementary Note 4. Polarization-resolved Raman measurements of unstrained WSe_2 and additional details on the fitting procedure of polarized data

Supplementary Note 5. Symmetry fingerprints of strained WSe_2 using polarized Raman.

Supplementary Note 1. Identification of the number of layers and description of straining setups.

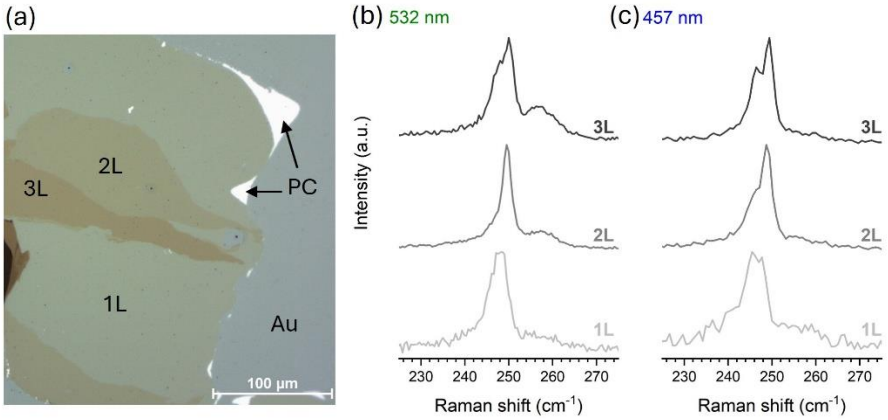

Figure S1. Identification of the number of layers in WSe_2 on Au. (a) Optical image of WSe_2 flakes and (b,c) unpolarized Raman spectra of 1L, 2L, and 3L WSe_2/Au samples under 532 nm and 457 nm excitations, respectively.

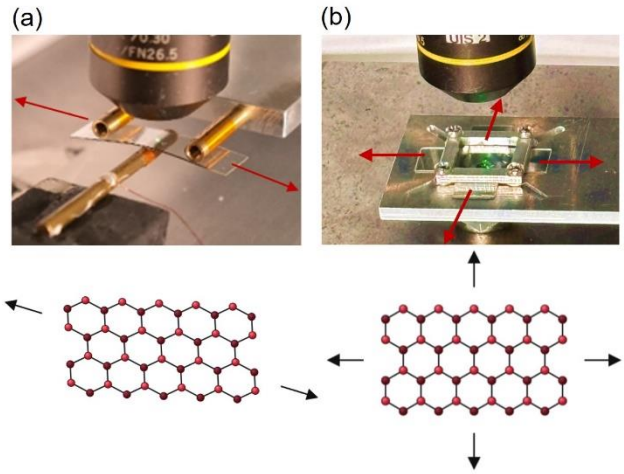

Figure S2. Experimental setups used for uniaxial and biaxial strain measurements and respective deformations of the WSe_2 crystal lattice. (a) Custom three-point bending platform employed for uniaxial strain experiments. (b) Cruciform bending stage used to apply biaxial strain. Red arrows indicate the direction of the applied mechanical deformation. The schematic representations of the WSe_2 crystal lattice were created using Inkscape.

Supplementary Note 2. Symmetry framework and Raman selection rules.

The polarization-resolved Raman measurement setup is illustrated in Figure S3. The angular dependence of the Raman intensity as a function of sample rotation angle can be calculated through the expression $I(\theta) \propto |\boldsymbol{e}_s \cdot R \cdot \boldsymbol{e}_i|^2$, where R is the Raman tensor of each Raman-active mode.[1]

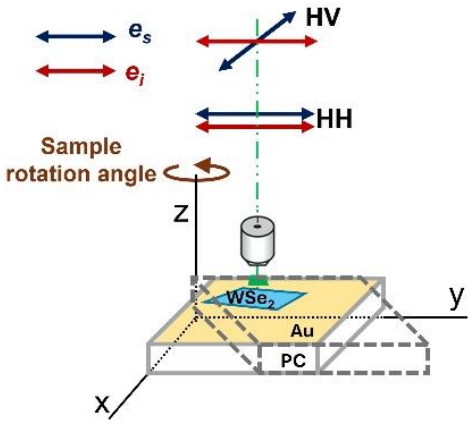

Figure S3. Schematic of polarized Raman setup for parallel (HH) and crossed (HV) configurations. The sample, consisting of WSe_2 layers on Au supported on a flexible polycarbonate (PC) substrate, is placed at the center of a rotation stage, while the incident (e_i) and scattered (e_s) electric-field vectors of light are kept fixed.

The symmetry groups, corresponding symmetry elements, and irreducible representations of the Raman-active vibrational modes considered throughout this work are summarized in Tables S1 and S2. In particular, the evolution from D_{3d}/D_{3h} symmetry toward lower-symmetry configurations induced by substrate interaction or uniaxial strain is reflected in the splitting and transformation of the in-plane doubly degenerate modes and the modification of the Raman selection rules. While freestanding monolayer WSe_2 belongs to the D_{3h} point group, the interaction with the Au substrate removes the horizontal mirror symmetry associated with the out-of-plane direction, resulting in an effective C_{3v} symmetry description for the supported layer.[2]

Table S1. Point groups and corresponding symmetry elements for the different WSe_2-based systems analyzed in this work. Here, C_n denotes an n-fold rotation axis. S_n is an improper rotation axis, σ_h (σ_v) a horizontal (vertical) mirror plane, i the inversion center and E the identity operation.

Material/system	**Point group**	**Symmetry elements**
Bulk 2H WSe_2	D_{6h}	C_6, C_3,C_2, $C_2^{'}$ S_6, S_3 i, σ_v, σ_d, σ_h E
2H WSe_2 (2n layer)	D_{3d}	C_3,C_2, S_6, i, σ_v, E
2H WSe_2 (2n+1 layer)	D_{3h}	C_3,C_2, S_3, σ_h, σ_v, E
WSe_2/Au	C_{3v}	C_3, σ_v, E
WSe_2 under uniaxial strain along mirror plane	C_s	σ_v, E
WSe_2 under arbitrary uniaxial strain	C_1	E

Table S2. Symmetry classification of the in-plane doubly degenerate and out-of-plane vibrations of WSe_2 for different symmetry groups. The irreducible representations are given according to the character tables of each point group**.**

Physical vibration	D_{3d}	D_{3h}	C_{3v}	C_s	C_1
In-plane mode	E_{2g}	E'	E	$A' + A''$	$A + A$
Out-of-plane mode	A_{1g}	A_1'	A_1	A'	A

The Raman tensors determine the angular dependence of the scattered intensity under sample rotation and therefore provide a direct link between lattice symmetry and polarization-resolved Raman fingerprints.

Considering that WSe_2 layers on Au substrates adopt the C_{3v} point group [2], the Raman-active in-plane (E) and out-of-plane (A_1) modes are described by the following Raman tensors:

$$R(A_1) = \begin{pmatrix} a & 0 & 0 \\ 0 & a & 0 \\ 0 & 0 & b \end{pmatrix} \quad (S1)$$

$$R(E_x) = \begin{pmatrix} c & 0 & 0 \\ 0 & -c & 0 \\ 0 & 0 & 0 \end{pmatrix}, \; R(E_y) = \begin{pmatrix} 0 & c & 0 \\ c & 0 & 0 \\ 0 & 0 & 0 \end{pmatrix} \quad (S2)$$

Under uniaxial strain, the symmetry is reduced, leading to lifting of the E mode degeneracy and modification of the Raman selection rules.

Note that E mode is doubly degenerate and therefore described by two tensors. The calculated angular Raman intensities of the in-plane and out-of-plane contributions under HH and HV configurations are isotropic,

$$I_{HH,A_1} \propto \text{constant} \quad (S3)$$

$$I_{HV,A_1} = 0 \quad (S4)$$

$$I_{HH,E} \propto \text{constant} \quad (S5)$$

$$I_{HV,E} \propto \text{constant} \quad (S6)$$

Under uniaxial deformation, a symmetry breaking is expected, and the double degeneracy of the in-plane mode is lifted.[3,4] Depending on the direction of the deformation, the symmetry-lowering occurs either to the C_s point group, if the strain axis is aligned with a crystallographic mirror plane of the crystal lattice, or to the C_1 point group, if the strain is applied along a general in-plane direction that does not preserve any mirror symmetry.

For C_s point group, the doubly degenerate in-plane E mode splits into A′ and A″ modes, while the out-of-plane A_1 mode transforms into an A′ mode. These new symmetry modes have the following Raman tensors:

$$R(A') = \begin{pmatrix} a & 0 & d \\ 0 & b & 0 \\ d & 0 & c \end{pmatrix} \quad (S7)$$

$$R(A'') = \begin{pmatrix} 0 & e & 0 \\ 0 & 0 & f \\ e & f & 0 \end{pmatrix} \quad (S8)$$

With this symmetry-lowering, the calculated Raman mode intensities as a function of the sample rotating angle become strongly anisotropic,

$$I_{HH,A'} \propto \left| \frac{a+b}{2} + \frac{a-b}{2} \cos 2\theta \right|^2 \quad (S9)$$

$$I_{HV,A'} \propto |\sin 2\theta|^2 \quad (S10)$$

$$I_{HH,A''} \propto |\sin 2\theta|^2 \quad (S11)$$

$$I_{HV,A''} \propto |\cos 2\theta|^2 \quad (S12)$$

For C_1 point group, both in-plane and out-of-plane modes transform into A modes,

$$R(A) = \begin{pmatrix} a & d & e \\ d & b & f \\ e & f & c \end{pmatrix} \quad (S13)$$

For this case, the Raman-active modes follow the angular intensity dependence given by

$$I_{HH,A} \propto \left| \frac{a+b}{2} + \frac{a-b}{2} \cos 2\theta + d \sin 2\theta \right|^2 \quad (S14)$$

$$I_{HV,A} \propto \left| d \cos 2\theta + \frac{a-b}{2} \sin 2\theta \right|^2 \quad (S15)$$

Contrary to the higher symmetric point group (C_{3v}), for both C_s and C_1 point groups, the out-of-plane Raman contribution is no longer forbidden for all angles in the HV configuration, therefore, the emergence of a non-zero out-of-plane Raman contribution under crossed polarization constitutes a direct experimental fingerprint of strain-induced symmetry lowering, and it can be used as a direct experimental probe to distinguish between unstrained/biaxial and uniaxial strain.

Figure S4 shows the angular dependence of the Raman-active modes intensity, considering the three possible symmetry groups, for the two polarization configurations: parallel (HH) and crossed (HV).

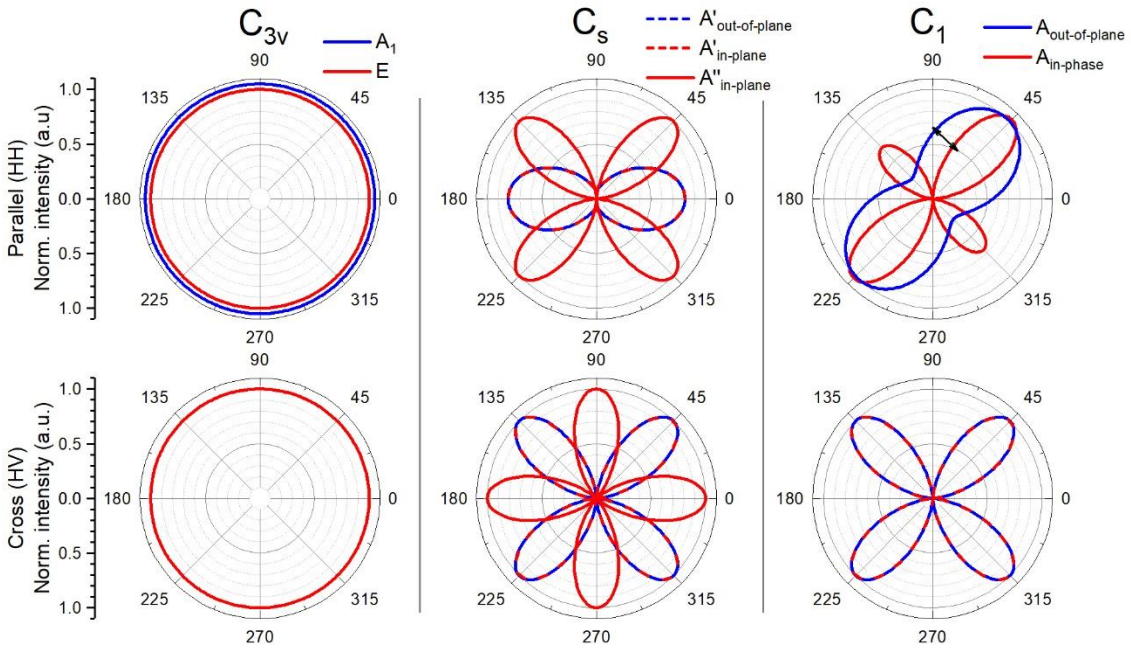

Figure S4. Simulation of polar plots under parallel (HH) and cross (HV) polarization configurations derived from Raman tensor analysis for in-plane and out-of-plane modes, assuming the different possible crystallographic symmetries of WSe_2. C_{3v} corresponds to unstrained and biaxial strain and two possible symmetry reductions C_s/C_1 can be induced by uniaxial strain. When the strain is applied along a mirror plane (C_s) and when the strain applied along an arbitrary direction (C_1). In-plane modes are represented by red lines and out-of-plane modes by blue lines. For the C_s, besides the color indicating in/out-of-plane modes, the mode symmetry is also represented by solid lines in the case of A'' and dashed line for A' modes. For the C_1 symmetry in the HH configuration, the two in-plane mode have similar angular dependence, being represented by one red curve.

Important to note that each phonon possesses its own Raman tensor. Under HH configuration for C_1 point group, the three Raman-active modes, although sharing the same symmetry, have

different tensor elements. In Figure S4 it is illustrated how the angular dependence can vary depending on the Raman tensor values, even when the mode symmetry remains the same.

As presented in the main text, the angular dependence observed in our experimental results under uniaxial strain is consistent with the predictions for the C_1 point group. Therefore, the applied uniaxial strain is oriented along a generic direction that does not coincide with any mirror plane.

Supplementary Note 3. Additional strain-dependent unpolarized Raman measurements for 1-3L WSe_2.

Additional unpolarized Raman spectra for 1L and 2L WSe_2 under strain are presented in Figure S5 and S6. The overall symmetry behavior remains unchanged across different layer numbers. The 3L WSe_2 was chosen to be presented in the main text because it provides access to larger strain values together with enhanced Raman intensity. Moreover, the influence of the metal substrate is more pronounced for 1L and 2L regions and that the 3L spectrum more closely reflects the intrinsic response of WSe_2 while still allowing efficient strain transfer.

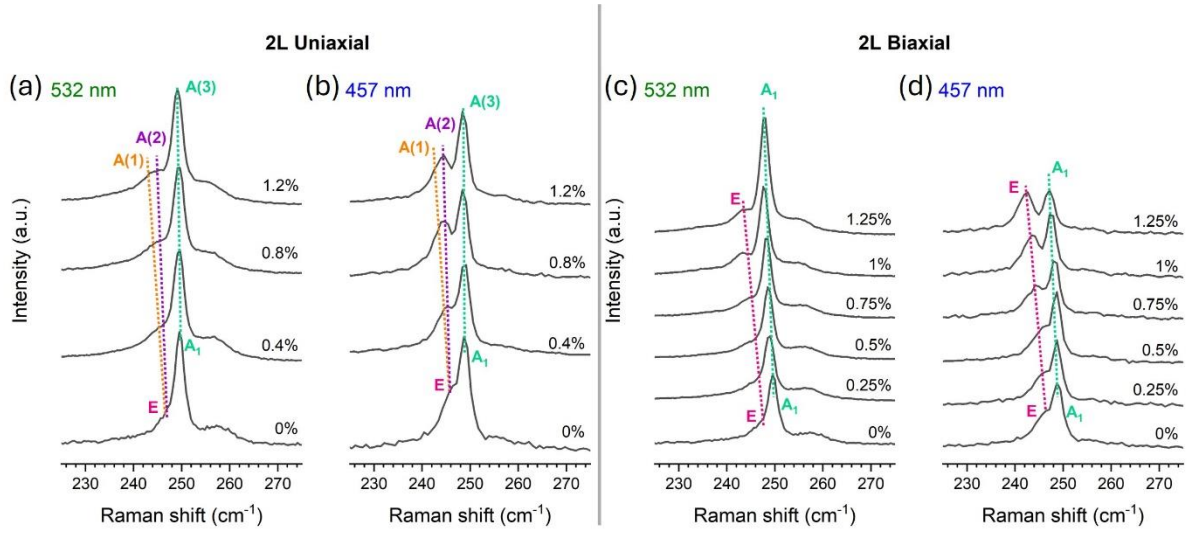

Figure S5. Unpolarized Raman spectrum of 2L WSe_2 using 532 and 457 nm excitation under external applied strain (a,b) Raman spectrum under increasing uniaxial strain up to 1.2%. (c,d) Raman spectra under increasing biaxial strain up to 1.25%. Dotted lines are used as guides to the eye to better visualize the evolution of the Raman modes with the applied strain. Pink and green lines indicate the in-plane (E) and out-of-plane (A_1) modes, respectively. Due to the reduced symmetry induced by uniaxial strain, the in-plane E mode splits into two components, A(1) (orange line) and A(2) (purple line), and the out-of-plane A_1 becomes A(3).

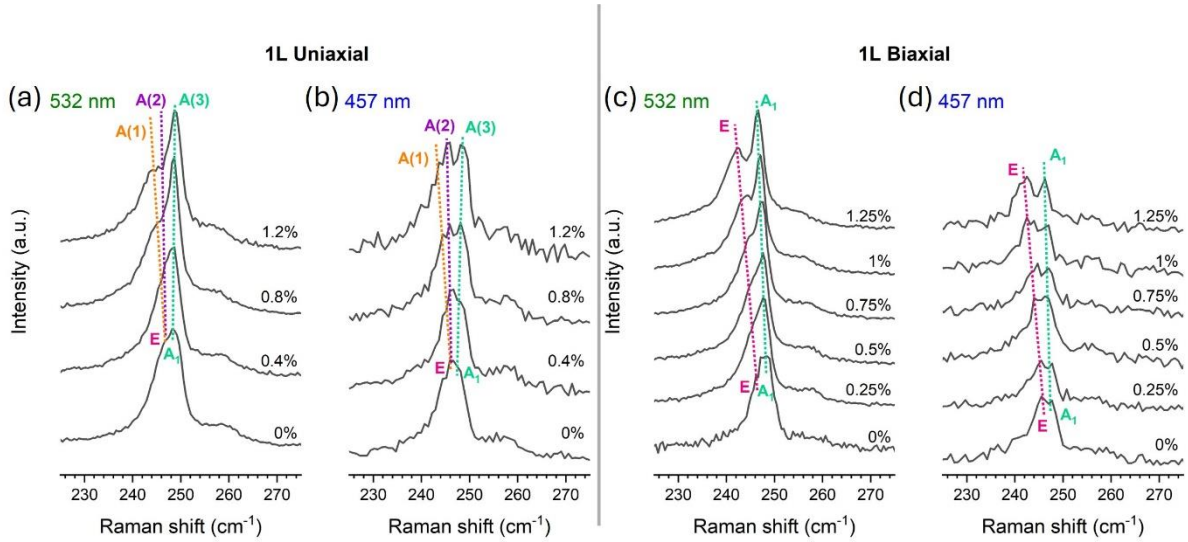

Figure S6. Unpolarized Raman spectrum of 1L WSe_2 using 532 and 457 nm excitation under external applied strain (a,b) Raman spectrum under increasing uniaxial strain up to 1.2%. (c,d) Raman spectra under increasing biaxial strain up to 1.25%. Dotted lines are used as guides to the eye to better visualize the evolution of the Raman modes with the applied strain. Pink and green lines indicate the in-plane (E) and out-of-plane (A_1) modes, respectively. Due to the reduced symmetry induced by uniaxial strain, the in-plane E mode splits into two components, A(1) (orange line) and A(2) (purple line), and the out-of-plane A_1 becomes A(3).

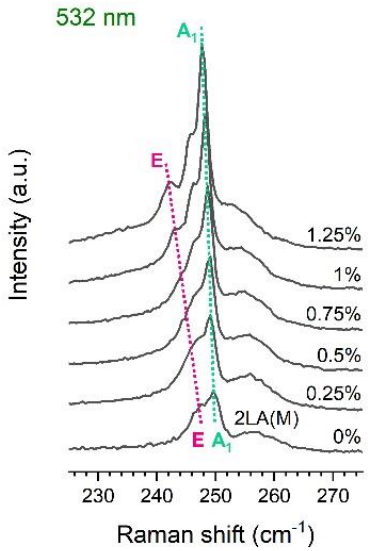

Figure S7. Unpolarized Raman spectrum of 3L WSe_2 using 532 under external applied biaxial strain. Dotted lines are used as guides to the eye to better visualize the evolution of the Raman modes with the applied strain. Pink and green lines indicate the in-plane (E) and out-of-plane (A_1) modes, respectively.

Supplementary Note 4. Polarization-resolved Raman measurements of unstrained WSe_2 and additional details on the fitting procedure of polarized data.

Figures S8a and S8b show the angular Raman response in the unstrained state of the in-plane modes together with the out-of-plane contribution acquired under HH and HV configurations, respectively. Polarization-resolved Raman spectra acquired in the unstrained state are also presented in Figures S8c and S8d. The Raman response exhibits the expected isotropic behavior upon sample rotation.

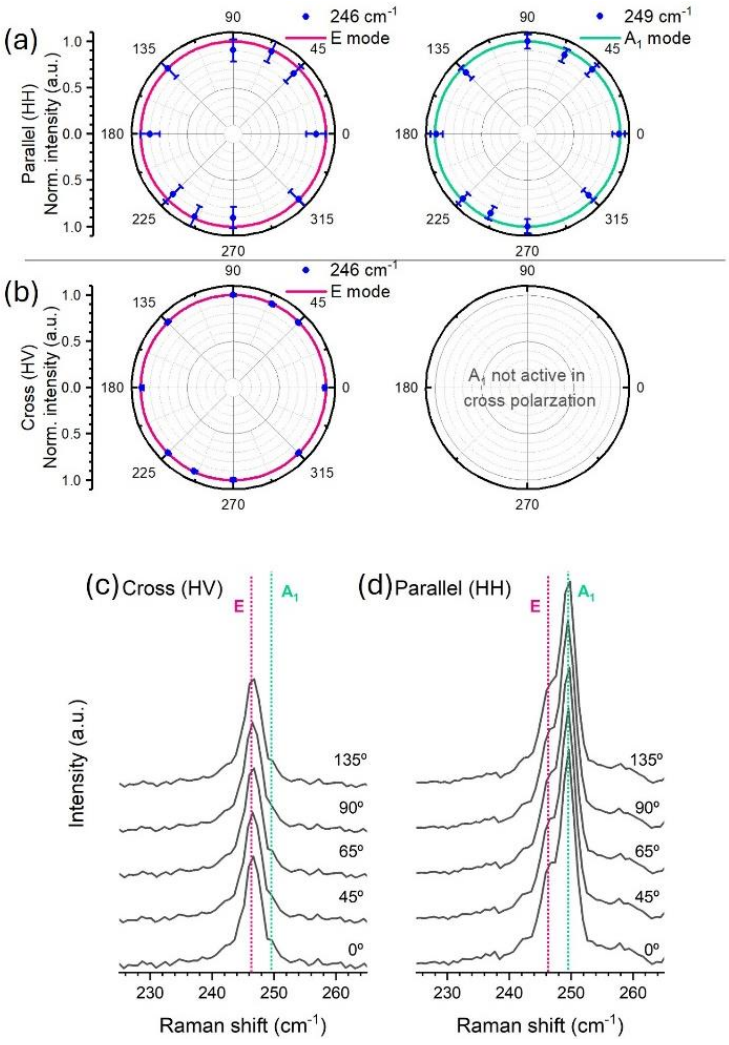

Figure S8. Polarization-resolved Raman response of unstrained 3L WSe_2 using 457 nm excitation. (a,b) Polar plots acquired under parallel (HH) and cross (HV) polarization configurations for the in-plane modes and the out-of-plane contribution. (c,d) Angle-dependent Raman spectra acquired under HV and HH configurations, respectively, during sample rotation. Dotted lines are used as guides to the eye to better visualize the position of the Raman modes. Pink and green lines indicate the in-plane (E) and out-of-plane (A_1) modes, respectively.

Representative Lorentzian fits of the Raman spectra under uniaxial and biaxial strain are shown in Figures S9 and S10, respectively. Under uniaxial strain, the spectra were decomposed into three main Lorentzian components, A(1), A(2), and A(3), corresponding to the two components arising from the splitting of the in-plane E mode and the out-of-plane A_1 mode, respectively. Additional weak components labelled "sup." were included in some HH spectra to account for minor spectral contributions and reproduce weak spectral shoulders. These supporting components are not assigned to additional strain-induced phonon modes. For the main components, the frequency, linewidth, and amplitude were generally allowed to vary freely, while in a limited number of strongly overlapping spectra one parameter was fixed to ensure a stable decomposition.

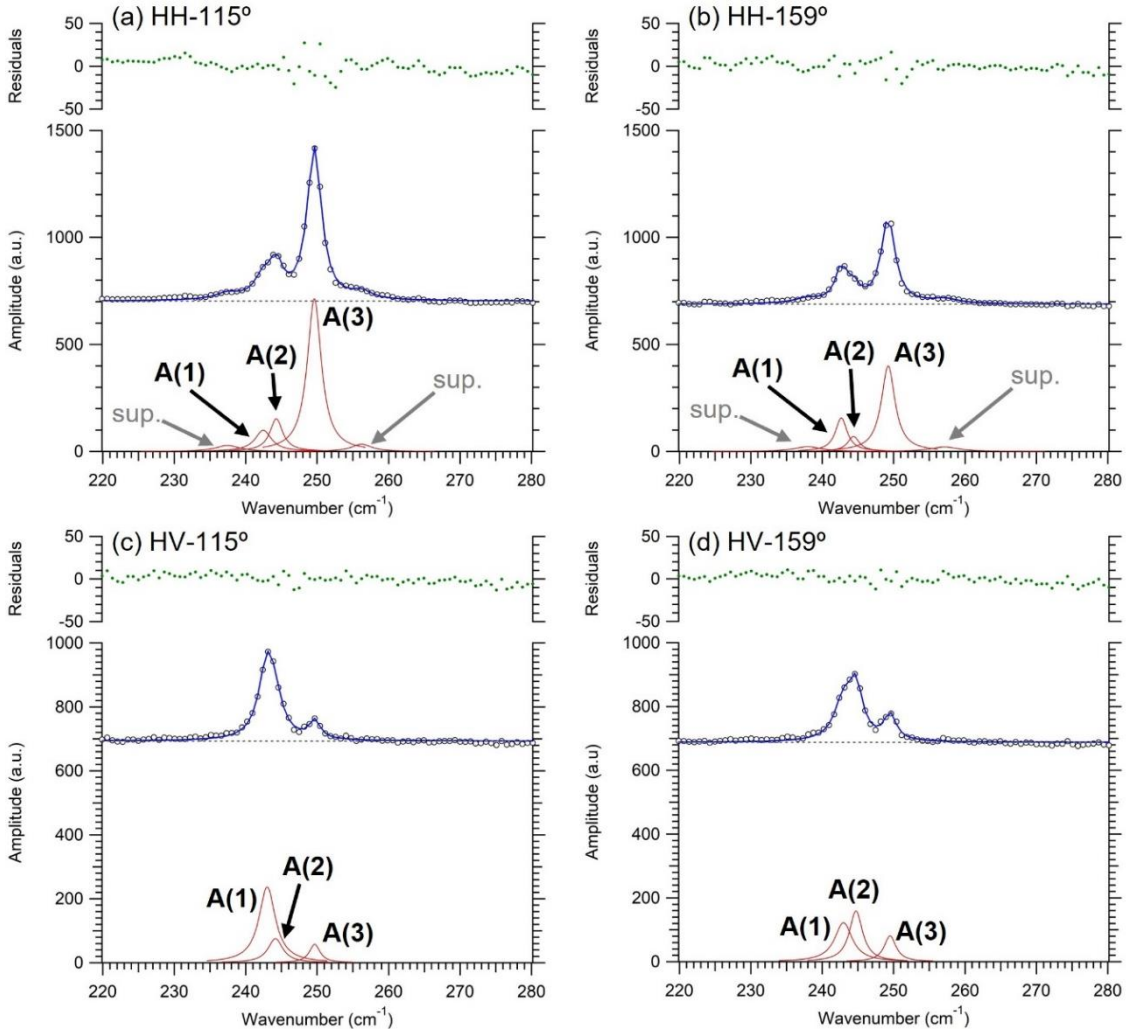

Figure S9. Representative Lorentzian fits of the polarized Raman spectra under uniaxial strain in the HH and HV polarization configurations at rotation angles of (a,c) 115º and (b,d) 159º. Experimental Raman spectra are shown as open circles, individual Lorentzian components as red solid lines, total fit as a blue solid line, and fitting residuals as green points. The individual Lorentzian components are assigned to the A(1), A(2) and A(3) phonon modes, plus to two additional supporting modes. The horizontal dashed line indicates the fitted background level.

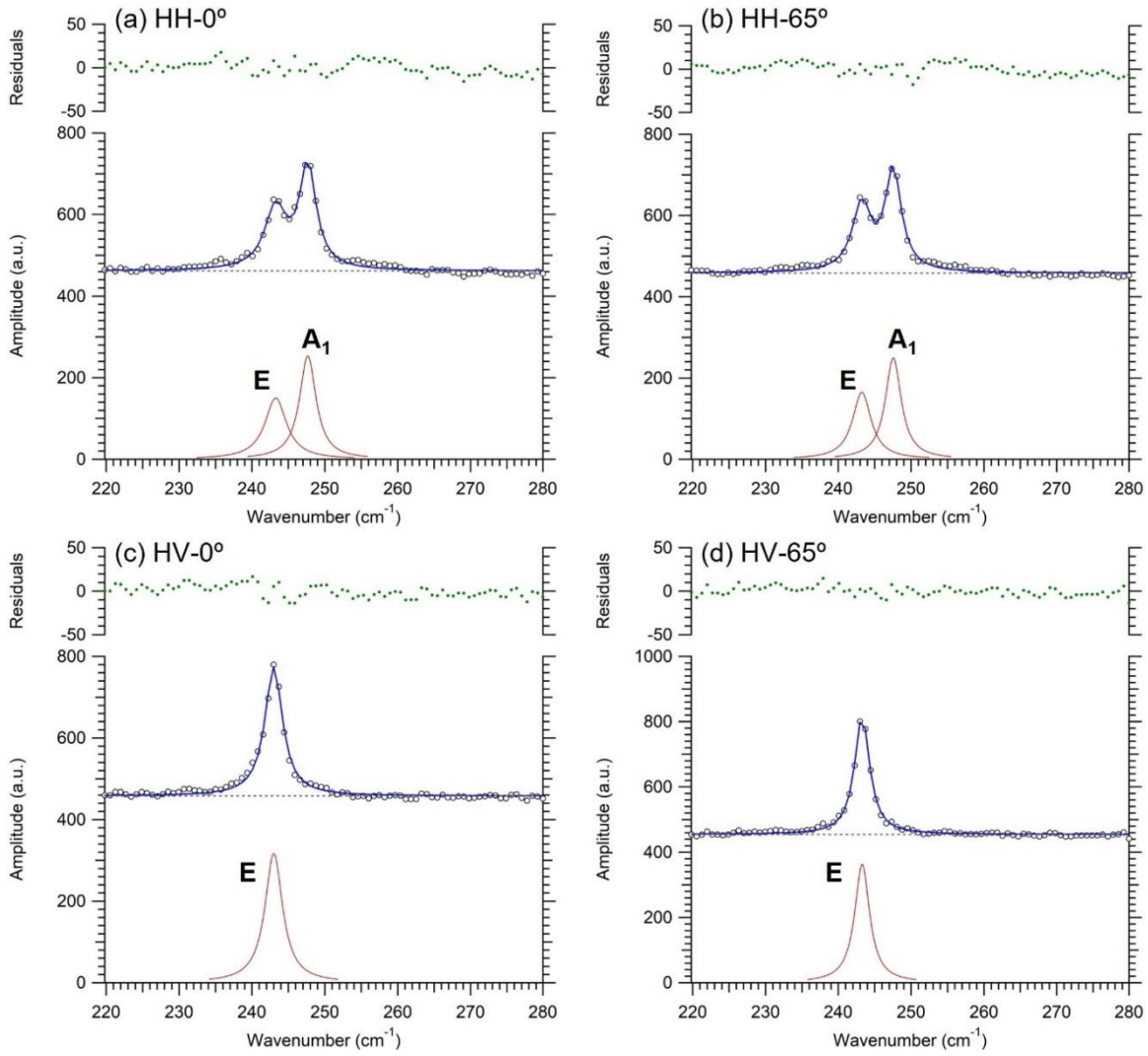

Figure S10. Representative Lorentzian fits of the polarized Raman spectra under biaxial strain in the HH and HV polarization configurations at rotation angles of (a,c) 0º and (b,d) 65º. Experimental Raman spectra are shown as open circles, individual Lorentzian components as red solid lines, total fit as a blue solid line, and fitting residuals as green points. The individual Lorentzian components are assigned to the E and A1 phonon modes. The horizontal dashed line indicates the fitted background level.

Supplementary Note 5. Symmetry fingerprints of strained WSe_2 using polarized Raman.

The symmetry fingerprints associated with the strain geometry of 3L are expected to be the same in 1L WSe_2. Figure S9 compares the unpolarized and polarized Raman response of uniaxial and biaxial strains in 1L WSe_2. Besides the splitting of the in-plane mode under uniaxial deformation, a non-zero intensity of the out-of-plane mode in the HV configuration is also observed, in contrast to the suppressed intensity of the same mode under biaxial deformation.

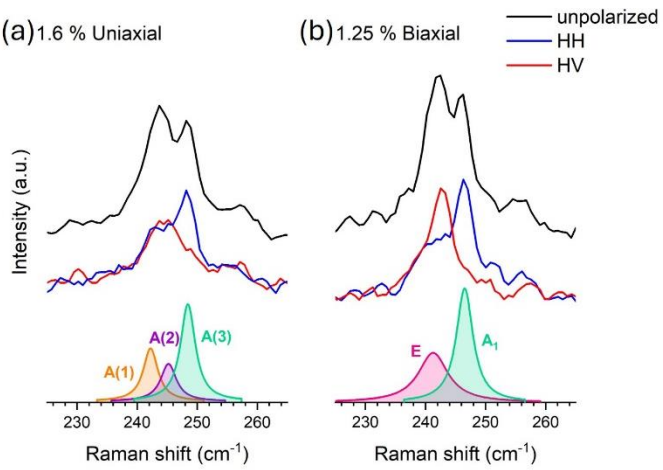

Figure S11. Unpolarized and polarized Raman response of 1L-WSe_2 under strain. (a) uniaxial and (b) biaxial deformation, using 457 nm excitation. The deconvolution of the Raman contributions is also shown, considering the C_1 and the C_{3v} point groups, for uniaxial and biaxial strain, respectively.

Figure S12 summarizes the Raman shifts extracted from the unpolarized spectra as a function of strain. Under uniaxial strain, Figure S10(a), the two in-plane components A(1) and A(2) can be clearly resolved only above approximately 1% strain. At lower strain, the spectral overlap between the two components prevents their independent contributions from being fully resolved. This is also reflected in the extracted Raman shifts, where the data points between 0 and 1% do not follow either of the linear trends defined by the resolved A(1) and A(2) modes. Instead, these apparent shifts reflect the combined contributions of the overlapping A(1) and A(2) components. Above ~1% strain, the two components become progressively separated and their individual shift rates can be reliably determined.

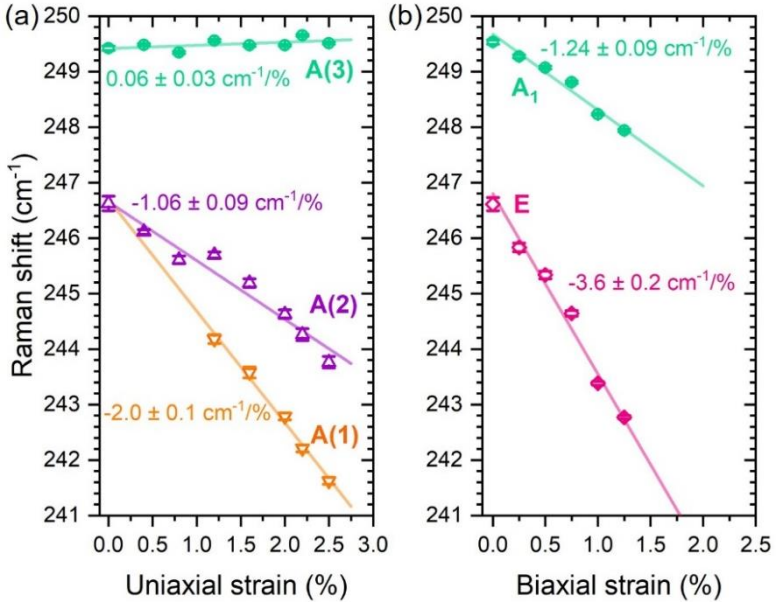

Figure S12. Raman shifts as a function of the applied strain. (a) uniaxial and (b) biaxial for 3L WS_2. The Raman shifts were obtained from fitting the unpolarized spectra of Figure 1(b) and Figure 3(a), measured with 457 nm excitation. The respective shift rates indicated in the figure for each mode are obtained from the slope of the linear fits.

References

[1] Kim J, Lee J and Cheong H Polarized Raman spectroscopy for studying two-dimensional materials *J. Phys. Condens. Matter* **32** 343001 (2020)

[2] Rodriguez A, Velický M, Řáhová J, Zólyomi V, Koltai J, Kalbáč M and Frank O Activation of Raman modes in monolayer transition metal dichalcogenides through strong interaction with gold *Phys. Rev. B* **105** 195413 (2022)

[3] Dadgar A M, Scullion D, Kang K, Esposito D, Yang E H, Herman I P, Pimenta M A, Santos E-J G and Pasupathy A N Strain Engineering and Raman Spectroscopy of Monolayer Transition Metal Dichalcogenides *Chem. Mater.* **30** 5148–55 (2018)

[4] Desai S B, Seol G, Kang J S, Fang H, Battaglia C, Kapadia R, Ager J W, Guo J and Javey A Strain-Induced Indirect to Direct Bandgap Transition in Multilayer WSe2 *Nano Lett.* **14** 4592–7 (2014)